

Two levels of topology in skyrmion lattice dynamics

Daniel Schick ¹, Markus Weißenhofer ^{1,2,3}, Levente Rózsa ^{1,4,5}, Jan Rothörl ⁶, Peter Virnau ⁶ and Ulrich Nowak ¹

¹*Fachbereich Physik, Universität Konstanz, DE-78457 Konstanz, Germany*

²*Department of Physics and Astronomy, Uppsala University, P. O. Box 516, S-751 20 Uppsala, Sweden*

³*Department of Physics, Freie Universität Berlin, Arnimallee 14, DE-14195 Berlin, Germany*

⁴*Department of Theoretical Solid State Physics, Institute of Solid State Physics and Optics, HUN-REN Wigner Research Centre for Physics, H-1525 Budapest, Hungary*

⁵*Department of Theoretical Physics, Budapest University of Technology and Economics, H-1111 Budapest, Hungary*

⁶*Institut für Physik, Johannes Gutenberg-Universität Mainz, DE-55122 Mainz, Germany*



(Received 17 May 2023; revised 11 September 2023; accepted 8 November 2023; published 25 January 2024)

Skyrmions are localized, topological spin structures that can be described as quasiparticles. Skyrmions in thin films are an ideal model system to study Brownian motion and lattice formation in two dimensions. They follow an equation of motion, the Thiele equation, which includes a topology-dependent chiral term, linear in velocity, causing a skyrmion Hall effect and a drastic reduction of the diffusion coefficient for individual skyrmions, as compared to normal Brownian particles. Using Brownian dynamics simulations, we show that this topological suppression of the diffusion can be partially lifted in two-dimensional lattices of skyrmions. Counterintuitively, this causes enhanced diffusive properties with increasing particle density, similar to odd-diffusive Brownian particles. We show how the topological charge of the skyrmions influences the dynamics of topological lattice defects, which also affects the dynamics of the phase formation.

DOI: [10.1103/PhysRevResearch.6.013097](https://doi.org/10.1103/PhysRevResearch.6.013097)

I. INTRODUCTION

Topology is a concept that defines quantities which remain invariant under continuous deformations of an object. Concepts of topology have been successfully applied in many areas of physics, ranging from, e.g., classical mechanics (Foucault pendulum) through cosmology and particle physics (Kibble-Zurek mechanism) to polymer physics (knots), as well as transport phenomena (quantum Hall effect) and topological defects (solitons) in condensed matter [1–6]. Two-dimensional representatives of the latter include topological lattice defects associated with the melting dynamics in two dimensions [7] and topological magnetic textures called skyrmions [8].

Magnetic skyrmions are localized topological spin structures, where the spin directions span the entire unit sphere [9–11]. They exhibit quasiparticle dynamics, are easily displaced when applying electric currents, and can be individually created and deleted [12,13]. Therefore, they have emerged as promising candidates for realizing novel spintronic devices [14–16] and applications based on the stochastic dynamics of skyrmions have been conceived for probabilistic computing [17,18], Brownian reservoir computing [19] and token-based computing [20].

The topological charge of skyrmions plays a crucial role in their dynamics. The Thiele equation [21] describes skyrmion

dynamics on the quasiparticle level, where the topology leads to a chiral term, linear in skyrmion velocity, typically referred to as *gyrocoupling*. This chiral term is responsible for the emergence of the skyrmion Hall effect, the transverse motion of skyrmions when driven by electric currents [22,23], and for the drastic reduction of their diffusion coefficient, as compared to normal Brownian particles [24], an effect that is called topological suppression of diffusion.

Skyrmions in thin films can form lattices strictly confined in two dimensions [25,26]. As such, they are ideal candidates [27,28] for studying Brownian dynamics, and phase transitions in two dimensions, which are otherwise difficult to observe [29–33]. Two-dimensional melting can be described within the Kosterlitz-Thouless-Halperin-Nelson-Young (KTHNY) theory [7,34–36]. This theory separates the melting of two-dimensional crystals into two distinct phase transitions, which are associated with the unbinding of lattice defects, the disclinations, dislocations, and dislocation pairs, with the former two being topological in nature. The dissociation of dislocation pairs into individual dislocations is associated with the quasicrystalline to hexatic transition, whereas the dislocations dissociating into disclinations mark the hexatic to isotropic liquid transition. The hexatic phase is notable for having quasi-long-ranged sixfold orientational correlations, despite the translational correlations being short ranged. While there has been extensive research on such phase transitions and defect dynamics in colloids [37–40], it remains to be discovered how the dynamics of these phase transitions are modified if the constituents of the lattice are chiral.

In this paper, we investigate the role of the topological charge of skyrmions on the dynamics of lattice defects in their ensembles. We study the skyrmions via Brownian dynamics

Published by the American Physical Society under the terms of the [Creative Commons Attribution 4.0 International](https://creativecommons.org/licenses/by/4.0/) license. Further distribution of this work must maintain attribution to the author(s) and the published article's title, journal citation, and DOI.

simulations, regarding them as quasiparticles. We solve their equations of motion numerically at finite temperatures, including a skyrmion-skyrmion interaction potential to model two-dimensional lattice formation [28,41]. Surprisingly, we find that the diffusion of skyrmions can increase with increasing quasiparticle density, which means that the topological suppression of diffusion can be partially lifted in skyrmion ensembles. Furthermore, we show that the diffusion coefficient of the skyrmions correlates with the diffusion of the topological defects of the lattice, whose dynamics drive the freezing and melting processes according to KTHNY theory.

II. THEORY

The KTHNY theory builds the basis for understanding melting processes in two dimensions based on topological arguments [7]. The characteristics of the system phases can be captured using correlation functions. One typically considers the spatial orientation correlation function, defined as $g_6(r) = \langle \Psi_6^*(r) \Psi_6(0) \rangle$ [35], or the dynamical orientation correlation function [42]

$$g_6(t) = \langle \Psi_6^*(t) \Psi_6(0) \rangle \quad (1)$$

with the local bond-order parameter

$$\Psi_{6,j} = \frac{1}{n_j} \sum_k e^{-6i\theta_{jk}}, \quad (2)$$

where θ_{jk} is the angle of the bond connecting the particle j with a neighboring particle k relative to a reference direction. The number of neighbors of particle j is denoted by n_j , and can be found using Voronoi tessellation. The functions g_6 are a measure of the correlation of the local lattice orientation in space or time, respectively. The local lattice orientation is the orientation of the lattice around a particle formed by the neighboring particles. The decay of both the spatial and dynamical orientation correlation function can be used to determine the phase of a two-dimensional lattice.

Topological defects, where particles have a different number of neighbors, play an important role in determining the orientation correlation function, and thereby the phase of the system. Circular particles in two dimensions form a hexagonal lattice leading to close packing. Moving two next-nearest neighbors closer to each other results in two particles having seven neighbors and two particles having five neighbors, known as a dislocation pair. A dislocation is a pair of particles with five and seven neighbors, and its topology can be determined by encircling the defect along the particle bonds. If this loop contains an additional step along one direction compared to the other ones, this extra step is called the Burgers vector and describes the topology of this defect. The Burgers vector can be considered as a topological charge since dislocations can only annihilate when two of them with opposite Burgers vectors form a dislocation pair. An individual particle with five or seven neighbors surrounded by particles with six neighbors is called a disclination [33]. Those with five and seven neighbors have opposite topological charges, called bond angle in this context, which annihilate by forming a dislocation. Examples of these defects are shown in Fig. 1. The phase transition from the quasicrystalline to the hexatic phase is associated with unbinding dislocation pairs into individual

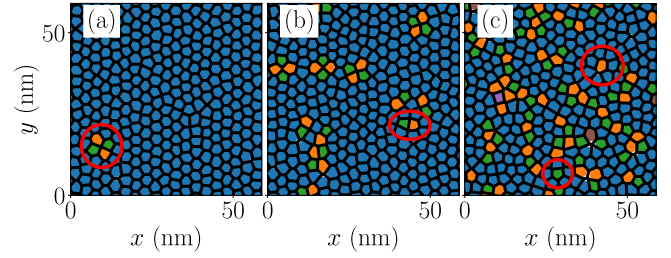


FIG. 1. Examples of topological defects in a lattice. Colors indicate number of neighbors according to Voronoi tessellation, five neighbors in green, six in blue, and seven in orange. Red circles highlight exemplary lattice defects: (a) a dislocation pair, (b) a topologically nontrivial dislocation, (c) topologically nontrivial disclinations with seven neighbors (upper), and with five neighbors (lower).

dislocations. These dislocations unbind into disclinations at the phase transition from the hexatic to the isotropic liquid phase [7].

The phase of the system is determined by static control parameters, such as the density and the temperature. The speed of the phase transition is governed by the creation, annihilation, and diffusive movement of the topological defects, which is influenced by the dynamics of the particles. Here, these particles are skyrmions characterized by a finite topological charge,

$$Q = \frac{1}{4\pi} \int \mathbf{S} \cdot (\partial_x \mathbf{S} \times \partial_y \mathbf{S}) d^2r, \quad (3)$$

where \mathbf{S} denotes the spin-vector field of unit length [8], and the integral is performed over the area of a skyrmion in the two-dimensional plane.

When this spin structure is treated as a quasiparticle, its equation of motion is known as the Thiele equation [21]

$$\mathbf{G} \times \mathbf{v}_i + \alpha \mathcal{D} \mathbf{v}_i = \mathbf{F}_i, \quad (4)$$

for the velocity \mathbf{v}_i of the skyrmion with index i . This equation is numerically solved using Heun's method for each skyrmion. We use the parameters $|\mathbf{G}|/k_B = 2.272 \text{ ns K nm}^{-2}$ and $\mathcal{D}/k_B = 3.396 \text{ ns K nm}^{-2}$ determined in Ref. [43], describing nanometer-sized skyrmions in a model system (Pt_{0.95}Ir_{0.05})/Fe/Pd(111) in an external magnetic field of 0.5 T.

In Eq. (4), the first term is the gyrocoupling term with the vector $\mathbf{G} = \mathcal{G} \mathbf{e}_\perp$ orthogonal to the plane in which the skyrmions move. For a discrete spin model, the magnitude of this vector is $\mathcal{G} = 4\pi Q \mu_s / (\gamma V_c)$, where μ_s is the spin magnetic moment, γ is the gyromagnetic ratio, and V_c is the size of the two-dimensional unit cell in the atomistic model of skyrmions. The vector \mathbf{G} is a result of the nontrivial topology of the skyrmion and causes a circular motion. For normal Brownian particles, such a term has been discussed in so-called odd-diffusive or odd-viscosity systems [44,45]. In the absence of this term, Eq. (4) becomes an overdamped Langevin equation describing normal Brownian motion.

The Thiele equation can be derived by applying a rigid-body approach to the microscopic equation of motion for the spin dynamics, the Landau-Lifshitz-Gilbert (LLG) equation.

That equation has two components, a precession around the effective field, and a relaxation towards that effective field. The latter is a damping term, the strength of which is given by the damping constant α . This magnetic damping leads to the second term in Eq. (4), where the dissipation tensor \mathcal{D} is

$$\mathcal{D}_{\mu\nu} = \frac{\mu_s}{\gamma V_c} \int \partial_\mu \mathbf{S} \cdot \partial_\nu \mathbf{S} d^2r, \quad (5)$$

with $\mu, \nu \in \{x, y\}$. For axially symmetric skyrmions considered here, the dissipation tensor is diagonal.

The vector $\mathbf{F}_i = \mathbf{F}_{i,\text{sk-sk}} + \mathbf{F}_{i,\text{th}}$ describes the force acting on the skyrmions. The effective skyrmion-skyrmion interaction term $\mathbf{F}_{i,\text{sk-sk}}$ is determined from a Lennard-Jones potential $U(r) = 4\epsilon[(\sigma/r)^{12} - (\sigma/r)^6]$. The well depth is $\epsilon/k_B = 8$ K, the size of the particle is $\sigma = 3.19$ nm and the cutoff distance of the potential is $r_{\text{cut}} = 10$ nm.

It has been shown that a Lennard-Jones potential with the given parameters can lead to a hexatic phase [46] similar to systems of purely repulsive disks [47]. Skyrmions in different systems may show different interaction potentials. In Ref. [48], a local minimum was found at short distances in the interaction potential between skyrmions in the present system, justifying the use of the Lennard-Jones potential. References [49,50] use decaying exponential interactions, while Ref. [28] uses a repulsive power law to model skyrmion-skyrmion interactions. The interaction potential between skyrmions is strongly influenced by the microscopic spin interactions in the system, but we confirmed that the qualitative conclusions from the simulations do not depend on whether the long-ranged decay is exponential or of the power-law form discussed here, as long as the skyrmion-skyrmion interaction is isotropic.

Diffusive skyrmion dynamics is modeled by stochastic forces with $\langle F_{i,\text{th},\mu} \rangle = 0$ and $\langle F_{i,\text{th},\mu}(t)F_{j,\text{th},\nu}(t') \rangle = 2\alpha k_B T \mathcal{D}_{\mu\nu} \delta_{ij} \delta(t - t')$ [43,51]. To analyze the diffusive motion we use the mean-square displacement (MSD)

$$\text{MSD}(t) = \langle [\mathbf{r}_i(t_0 + t) - \mathbf{r}_i(t_0)]^2 \rangle, \quad (6)$$

where \mathbf{r}_i is the position of the skyrmion with $\dot{\mathbf{r}}_i = \mathbf{v}_i$. For normal diffusion the MSD increases linearly with time and the diffusion coefficient is defined as $D = \lim_{t \rightarrow \infty} \text{MSD}(t)/(4t)$. From Eq. (4), the diffusion coefficient of a free skyrmion can be calculated as [24,51–53]

$$D = k_B T \frac{\alpha \mathcal{D}}{\mathcal{G}^2 + (\alpha \mathcal{D})^2}. \quad (7)$$

For nontrivial topology $\mathcal{G} \neq 0$, the low- α dependence is $D \propto \alpha$, whereas otherwise it is $D \propto 1/\alpha$, as for normal Brownian particles. As the free-diffusion coefficient with finite topological charge is much lower than with no topological charge, one speaks of topological suppression of diffusion [24].

This suppression can be understood as follows. According to Eq. (4), applying a force to a skyrmion causes it to move under an angle relative to the applied force. The velocity component perpendicular to the applied force is a consequence of the gyrocoupling, the component parallel to the force is governed by the dissipative term. The angle between the force and the velocity is called the skyrmion Hall angle $\theta = \arctan[\mathcal{G}/(\alpha \mathcal{D})]$ [23]. As mentioned above, the magnitude of the thermal force $\mathbf{F}_{i,\text{th}}$ is not influenced by the gyrocoupling \mathcal{G} since on infinitesimal timescales the gyroscopic

motion proceeds along equipotential lines perpendicular to the forces, meaning that it does not affect thermalization. However, the thermal force displaces the skyrmion by $\Delta x = F_{i,\text{th}}/\sqrt{\mathcal{G}^2 + (\alpha \mathcal{D})^2} \Delta t$, which is reduced due to the nontrivial topology of the skyrmion.

Interestingly, the topological suppression of diffusion can be lifted when the motion of the skyrmions is confined. The simplest example in this context is the motion along one axis with an one-dimensional harmonic potential limiting the motion perpendicular to that axis. Detailed analytical and numerical calculations are presented in Appendix A. At short times, the standard deviation of the skyrmion position from the deterministic path is given by Eq. (7) in both components along and perpendicular to the axis of unconfined movement. In the long-time limit, the MSD along the confined direction saturates and is no longer diffusive. While the motion along the unconfined direction remains diffusive, we observe that the diffusion coefficient increases,

$$D = \frac{k_B T}{\alpha \mathcal{D}}. \quad (8)$$

Here, the influence of the topological charge of the skyrmion vanishes. Since the diffusion increases, we call this phenomenon lifting of the topological suppression.

III. RESULTS

We now study the diffusive motion of interacting skyrmion ensembles by simulating 5016 skyrmions starting with thermalized skyrmion lattices at $T = 20$ K. We vary the skyrmion density and compare the diffusion for skyrmions with gyrocoupling \mathcal{G} present and absent to attribute emergent effects to the chiral motion of the skyrmions. For $\mathcal{G} = 0$, we use a damping constant of $\alpha = 0.1$, for $\mathcal{G} \neq 0$, we compare the cases of $\alpha = 0.1$ and 0.01 . Since not all simulated systems show a linear increase of MSD with time in the long-time limit of our simulation, calculating a diffusion constant is not possible. Instead, we calculate the MSD for a fixed time $t_1 = 16.19$ ns to compare the diffusion of skyrmion lattices with different densities. Figure 2 compares the resulting MSD for skyrmion ensembles with and without gyrocoupling. For low densities, all curves reach the limit of free diffusion given by Eq. (7). Without gyrocoupling, the diffusion decreases monotonously with increasing density and, especially for low densities, it decreases exponentially as has been shown theoretically for colloids [54]. For $\mathcal{G} \neq 0$, the skyrmion-skyrmion collisions lift the topological suppression, and the diffusion increases at small densities. This effect is analogous to the skyrmion diffusing in a one-dimensional harmonic potential. However, the diffusion of skyrmions with finite topological charge stays below the normal Brownian motion of particles with $\mathcal{G} = 0$, meaning that the topological suppression is only partially lifted. At higher densities, the restriction of the movement also observed without gyrocoupling becomes dominant, and the diffusion starts to decrease after a maximum. The maximum occurs at a lower density for the larger value of α .

When increasing the skyrmion density even further, one observes a transition into the quasicrystalline phase, where all three curves show a rapid decrease in MSD at the same threshold density, indicating that the phase of the system is

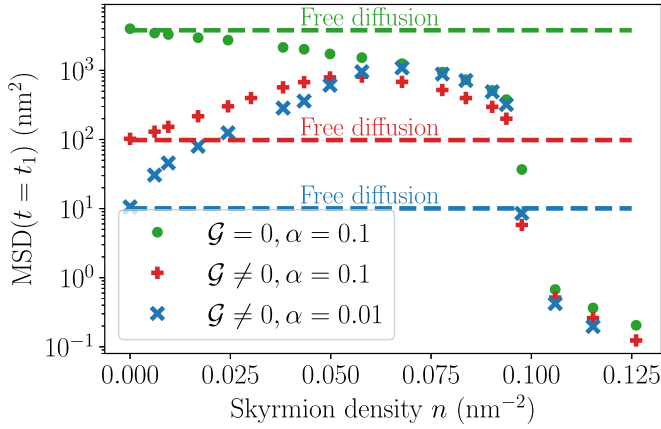


FIG. 2. Influence of the gyrocoupling on the diffusion of skyrmions. The MSD is calculated at time t_1 as a function of skyrmion lattice density n . Dashed lines show analytical values for free diffusion according to Eq. (7) multiplied with $4t_1$ to get the average MSD, using parameters from Ref. [43].

independent of the skyrmion dynamics. A calculation of the spatial correlation function $g_6(r)$ also shows no difference between curves of the same density and confirms the phase transition around the drop in MSD; see Appendix E for details. However, note that we could not resolve the hexatic phase with the chosen step size in density.

Enhanced self-diffusion in lattices of Brownian particles was recently predicted for odd-viscosity systems [44,45], and suggested to occur in skyrmionic systems [55]. In Ref. [45], it was also found that increasing the density causes a reduction of the Hall angle, confirming our finding that topological effects can be suppressed in skyrmion lattices. This suggests that the lifting of topological suppression depends on the ratio of $\mathcal{G}/(\alpha\mathcal{D})$, which is equal to $\tan\theta$ for free diffusion. We present a calculation of the skyrmion Hall angle in lattices based on our data in Appendix B, where we also find a drastic reduction with increased lattice density.

The dynamics of the individual particles plays also a critical role in understanding the movement of topological lattice defects shown in Fig. 1.

In Fig. 3, we analyze the MSD dynamics of these different types of topological defects numerically. We use a damping constant of 0.1, with the skyrmion density being $n = 0.09 \text{ nm}^{-2}$ and the temperature $T = 20 \text{ K}$. As indicated by the high MSD in Fig. 2, at these parameter values the system is in the isotropic liquid phase where all three types of topological defects are present. It is immediately clear that the gyrocoupling of the skyrmions reduces the diffusion compared to normal Brownian quasiparticles for all topological defects. This can be explained by the suppressed diffusion of skyrmions due to the gyrocoupling term and it shows that the diffusion of lattice defects is reduced by the topology of the skyrmions.

Irrespective of the constituents of the lattice, the MSD of the lattice defects increases with their size, i.e., dislocation pairs consisting of four skyrmions diffuse faster than dislocations, which are made of two skyrmions. This effect is in accordance with results found for colloids where larger defects such as dislocation pairs also diffuse faster [37,39].

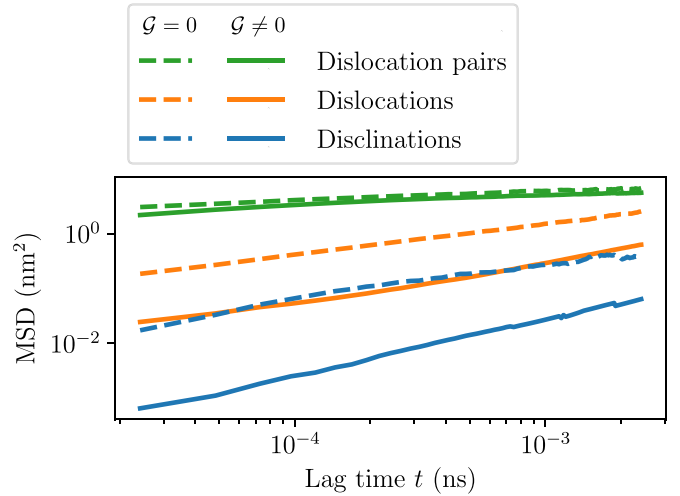


FIG. 3. Effect of the skyrmion topology on the thermal motion of lattice defects. The MSD is calculated for different topological defects in skyrmion lattices with and without gyrocoupling. Damping constant $\alpha = 0.1$, density $n = 0.09 \text{ nm}^{-2}$, and temperature $T = 20 \text{ K}$.

Since the diffusion for large defects is much faster than for the individual skyrmions, the diffusion is mediated by defects jumping between different clusters of skyrmions, with larger defects consisting of more skyrmions being able to jump easier. We observed a reduced number of jumps, and thus, reduced lattice defect diffusion as a consequence of the skyrmions' finite topological charge; see Appendix C.

In the MSD, it is also visible that larger defects show a more subdiffusive behavior, which is especially noticeable for dislocation pairs, where the increase of MSD with time is minimal. These observations show that lattice defects of different topologies differ in their diffusive behavior, indicating that both the topology of the lattice defect and the constituents are relevant in describing the defects' diffusion, having major implications for the dynamics of melting skyrmionic systems. It turns out that the topology of the constituents affects the dynamics of phase formation. This process is initially slower because of the topological suppression of the diffusion, but it speeds up as the number of collisions between the particles increases and the suppression is lifted. In Appendix D, we show melting and freezing processes, where we make use of orientational correlation functions and show the influences of topology on these systems.

IV. CONCLUSION

To conclude, we have studied the twofold impact of topology on skyrmion lattice dynamics by Brownian dynamics simulations of the stochastic Thiele equation. We showed that while the topology of skyrmions slows down their free diffusive motion, collisions with other skyrmions can lift this topological suppression of diffusion. Consequently, increasing the skyrmion lattice density enhances the mobility of the skyrmions for sufficiently low lattice densities, in analogy to what was recently discovered in odd-diffusive systems [44,45]. Additionally, we have revealed that the speed of the diffusive motion has a maximum at some intermediate density

that decreases for larger damping parameters, followed by a decline and a sudden drop at the phase transition into the solid phase.

The effect of topology on skyrmion diffusion further affects the diffusive properties of topological defects in the skyrmion lattice. The topological suppression of the diffusion of skyrmions decreases the diffusion rate of the corresponding lattice defects. Consequently, freezing and melting processes driven by the dynamics of these defects become slower due to the topological charge of the skyrmions.

Magnetic skyrmions in thin films are an ideal playground to study lattice formation in two dimensions, linking the field of spintronics with the physics of soft matter and phase transitions in low dimensions. Since the density of skyrmions and their interactions can be controlled by external magnetic fields [28], temperature and field sweeps will make it possible to study the dynamics of melting and freezing processes in detail, uncovering the role of the two levels of topological properties in skyrmion lattices experimentally.

ACKNOWLEDGMENTS

We acknowledge funding by the Deutsche Forschungsgemeinschaft (DFG, German Research Foundation) via SFB 1432 and Project No. 403502522 and SFB 1551 - Project No. 464588647, from TopDyn, by the Horizon Europe Project No. 101070290 (NIMFEIA), by the National Research, Development, and Innovation Office (NRDI) of Hungary under Projects No. K131938 and No. FK142601, by the Ministry of Culture and Innovation and the National Research, Development and Innovation Office within the Quantum Information National Laboratory of Hungary (Grant No. 2022-2.1.1-NL-2022-00004), by the Hungarian Academy of Sciences via a János Bolyai Research Grant (Grant No. BO/00178/23/11), and by the Young Scholar Fund at the University of Konstanz. We acknowledge fruitful discussions with M. Kläui.

APPENDIX A: SKYRMION DIFFUSION IN CONSTRAINED GEOMETRIES

In skyrmion lattices, the movement of any particular skyrmion is restricted by the presence of other skyrmions, which create a temporally varying nonhomogeneous energy landscape for said skyrmion. As we have shown in the main text using simulations, this nonhomogeneous energy landscape gives rise to the peculiar phenomenon that the diffusive motion of the skyrmions in lattices can be higher than the free diffusion. We attribute this to the fact that the *suppression of the diffusion by the gyrocoupling* [24] is itself, at least partially, lifted in skyrmion lattices.

While our line of reasoning in the main text is mostly qualitative (we draw parallels to existing literature on this [44,45,55]), we aim to provide a more quantitative explanation of the lifting of the suppression of the diffusion by performing analytical calculations in what follows. However, the temporally varying and complex nature of the energy landscape of a single skyrmion within a skyrmion lattice renders analytical calculations very complicated, so we consider a simpler system instead, i.e., we model a single skyrmion in a harmonic potential along one spatial direction. As demonstrated

below and in Refs. [56,57], this simple system allows for an unambiguous demonstration of the lifting of the diffusion suppression.

Without loss of generality, we assume that the harmonic potential reads as $U(x, y) = \kappa y^2/2$, with κ being the spring constant of the harmonic potential and x and y the position of the skyrmion. The emerging force is thus given by $\mathbf{F} = -\kappa y \mathbf{e}_y$. In matrix form, the stochastic Thiele equation [21] for such a force reads as

$$\begin{pmatrix} \alpha\mathcal{D} & -\mathcal{G} \\ \mathcal{G} & \alpha\mathcal{D} \end{pmatrix} \mathbf{v} + \begin{pmatrix} 0 & 0 \\ 0 & \kappa \end{pmatrix} \mathbf{r} = \mathbf{F}_{\text{th}}. \quad (\text{A1})$$

This expression can be cast into the form $\mathbf{v} = -\Omega \mathbf{r} + \sigma \mathbf{F}_{\text{th}}$ with Ω and σ being 2×2 matrices that read as

$$\Omega = \frac{\kappa}{(\alpha\mathcal{D})^2 + \mathcal{G}^2} \begin{pmatrix} 0 & \mathcal{G} \\ 0 & \alpha\mathcal{D} \end{pmatrix}, \quad (\text{A2})$$

$$\sigma = \frac{1}{(\alpha\mathcal{D})^2 + \mathcal{G}^2} \begin{pmatrix} \alpha\mathcal{D} & \mathcal{G} \\ -\mathcal{G} & \alpha\mathcal{D} \end{pmatrix}. \quad (\text{A3})$$

This is a linear stochastic equation of motion that has the formal solution [58]

$$\mathbf{r}(t) = e^{-\Omega t} \mathbf{r}(0) + \int_0^t e^{-\Omega(t-t')} \sigma \mathbf{F}_{\text{th}}(t') dt'. \quad (\text{A4})$$

The mean value and the second moments calculated from this expression read as

$$\langle \mathbf{r}(t) \rangle = e^{-\Omega t} \langle \mathbf{r}(0) \rangle, \quad (\text{A5})$$

$$\begin{aligned} \langle \mathbf{r}(t) \mathbf{r}(t)^\text{T} \rangle &= e^{-\Omega t} \langle \mathbf{r}(0) \rangle \langle \mathbf{r}(0) \rangle^\text{T} \\ &+ \left\langle \int_0^t e^{-\Omega(t-t')} \sigma \mathbf{F}_{\text{th}}(t') dt' \right. \\ &\times \left. \left(\int_0^t e^{-\Omega(t-t'')} \sigma \mathbf{F}_{\text{th}}(t'') dt'' \right)^\text{T} \right\rangle. \quad (\text{A6}) \end{aligned}$$

Note that we have used the fact that the mean value of the stochastic force vanishes.

Hereinafter, we assume that the skyrmion is initially located in the potential minimum, i.e., $y(0) = 0$. Moreover, since the system is invariant under translations along the x axis, we can set $x(0) = 0$ without loss of generality. As a consequence, $\langle \mathbf{r}(0) \rangle \equiv 0$ and the first term of the second moments vanishes.

Using the rules for matrix exponentials, we compute

$$e^{-\Omega t} = \begin{pmatrix} 1 & \frac{\mathcal{G}}{\alpha\mathcal{D}} \left(e^{-\kappa \frac{\alpha\mathcal{D}}{(\alpha\mathcal{D})^2 + \mathcal{G}^2} t} - 1 \right) \\ 0 & e^{-\kappa \frac{\alpha\mathcal{D}}{(\alpha\mathcal{D})^2 + \mathcal{G}^2} t} \end{pmatrix}. \quad (\text{A7})$$

Inserting this into the formula for the second moments and using the fact that $\langle \mathbf{F}_{\text{th}}(t) \mathbf{F}_{\text{th}}^\text{T}(t') \rangle = 2\alpha k_B T \mathcal{D} \mathbb{1} \delta(t - t')$, we get

$$\langle x^2(t) \rangle = 2 \frac{k_B T}{\alpha\mathcal{D}} \left[t + \frac{\mathcal{G}^2}{2\alpha\mathcal{D}\kappa} \left(1 - \left(2 - e^{-\kappa \frac{\alpha\mathcal{D}}{(\alpha\mathcal{D})^2 + \mathcal{G}^2} t} \right)^2 \right) \right], \quad (\text{A8})$$

$$\langle y^2(t) \rangle = \frac{k_B T}{\kappa} \left(1 - e^{-2\kappa \frac{\alpha\mathcal{D}}{(\alpha\mathcal{D})^2 + \mathcal{G}^2} t} \right). \quad (\text{A9})$$

Performing a Taylor expansion up to first order in time around $t = 0$, the above expressions reduce to the relations for free, two-dimensional Brownian motion, i.e., $\langle x^2(t) \rangle = \langle y^2(t) \rangle = 2k_B T \frac{\alpha \mathcal{D}}{(\alpha \mathcal{D})^2 + \mathcal{G}^2} t$. At longer timescales, $\langle y^2(t) \rangle$ converges to $k_B T / \kappa$ (this can also be obtained using the equipartition theorem), while $\langle x^2(t) \rangle$ increases linearly in time with a greatly increased diffusion coefficient that reads as

$$D^{\text{eff}} = \frac{k_B T}{\alpha \mathcal{D}}. \quad (\text{A10})$$

This effective diffusion coefficient for a skyrmion in a harmonic potential is the same as the one for a free Brownian particle in the absence of gyrocoupling. That is why we conclude that the presence of the potential effectively suppresses the impact of the gyrocoupling on Brownian motion at longer timescales, thus increasing the diffusive motion as compared to the free case, where the diffusion is reduced by the gyrocoupling. The fact that the diffusion suppression at low times is not lifted can be understood as follows: The absolute value of the velocity of a skyrmion as a consequence of a force F is $v = F / \sqrt{\mathcal{G}^2 + (\alpha \mathcal{D})^2}$, whether F is deterministic or stochastic. As the thermal force exerted on an individual skyrmion is independent of the gyrocoupling, the instantaneous velocity as a consequence of a force will always be lowered by the gyrocoupling. In other words, the mean-squared displacement for small time differences is always lowered by a finite \mathcal{G} .

In Fig. 4, we show the time-resolved data of the second moments of both the x and y directions for different choices of α . For the force, we used a value of $\kappa/k_B = 1 \text{ K nm}^{-2}$. For the x direction it is visible that after an initially lower diffusion, where skyrmions with high values of α diffuse faster, the skyrmions start to show superdiffusion, before diffusing normally again with a higher diffusion constant. For this increased diffusion constant, low α skyrmions show stronger diffusion than ones with high α . For the y direction, all skyrmions show a bounded MSD. The skyrmions diffuse normally until they reach this upper bound.

The validity of Eq. (A10) is demonstrated in Fig. 5, where we present the effective diffusion constant D^{eff} in the long-time limit as a function of the damping constant α . It is noticeable that the diffusion constant along the x axis is increased by orders of magnitude as compared to the one for free diffusion. Furthermore, $D^{\text{eff}} \propto 1/\alpha$, which is what one would expect for free diffusion of skyrmions with $\mathcal{G} = 0$. The free-diffusion constant for topologically nontrivial skyrmions is $D \propto \alpha$ for low values of α . In contrast to skyrmions within a harmonic potential, where the impact of the gyrocoupling on the diffusive motion is fully lifted, we find that for skyrmions in lattices the impact of gyrocoupling is still visible and thus only *partially lifted*. This is shown in Fig. 2 of the main text where simulations with and without the gyrocoupling term do not produce the same diffusion coefficient. We attribute this to the fact that the potential of a single skyrmion in a lattice is much more complex than the case considered above and that it is varying with time. Qualitatively, it can be understood as follows: As shown above, the presence of a potential along some axis leads to a reduction of the diffusion along this axis and a drastic enhancement along the perpendicular axis. Since the potential is constantly changing, the axes along which diffusive motion is increased or decreased are changing as

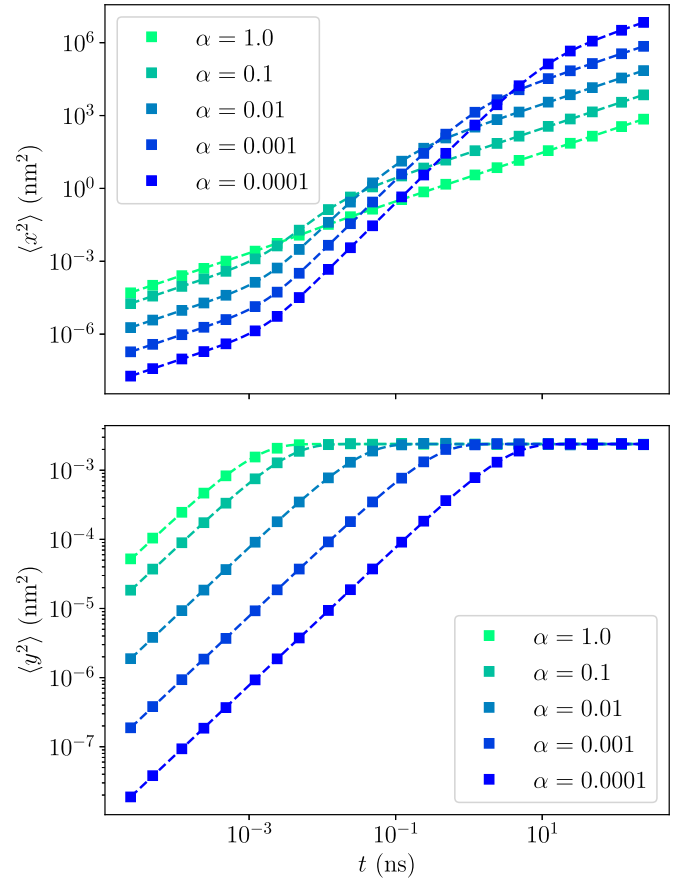


FIG. 4. Second moments $\langle x^2 \rangle$ and $\langle y^2 \rangle$ for skyrmion diffusion in a one-dimensional harmonic potential. Squares show data points, lines show the analytical curve according to Eqs. (A8) and (A9), respectively.

well. This means that the Brownian motion of some skyrmion along any given axis can be either increased or decreased, as compared to the free diffusion, depending on the current configuration of the neighboring skyrmions. On average, this can lead to an overall increase or decrease of the Brownian

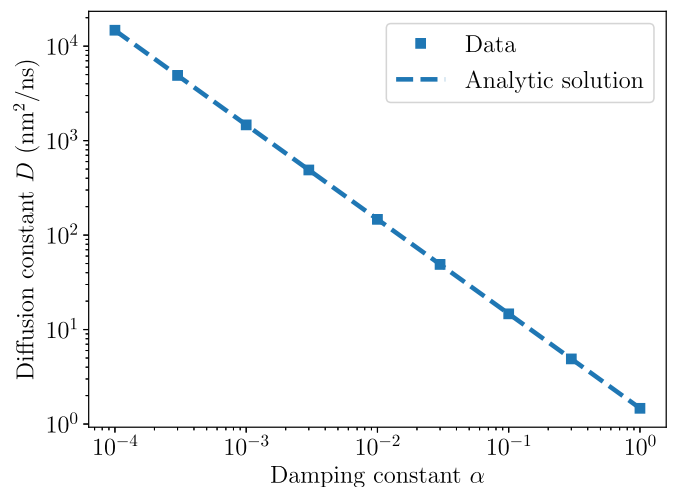


FIG. 5. Diffusion constant D^{eff} for a skyrmion constricted by a one-dimensional harmonic potential.

motion, depending on the average configuration of the neighboring skyrmions.

APPENDIX B: EFFECTIVE GYROCOUPLING AND SKYRMION HALL ANGLE

The diffusion of skyrmions in a lattice increases compared to free diffusion as presented in the main text. We explain this with the diffusion suppression by the gyromotion being lifted. We can assign an effective gyrocoupling $\tilde{\mathcal{G}}$ to skyrmions for describing the diffusive motion in lattices, which is strictly lower than the gyrocoupling in free-diffusive systems, indicating the suppression of topological properties. This allows us to calculate an effective skyrmion Hall angle in lattices. Due to a reduced effective gyrocoupling, we expect the skyrmion Hall angle to also diminish in magnitude in ensemble systems.

To calculate the effective skyrmion Hall angle in our system, we need to compare the diffusion constant in skyrmion systems with and without gyrocoupling present. Skyrmions with a nonzero gyrocoupling \mathcal{G} have a free-diffusion coefficient of [24,51–53]

$$D_{\mathcal{G}\neq 0} = k_B T \frac{\alpha \mathcal{D}}{\mathcal{G}^2 + (\alpha \mathcal{D})^2}, \quad (\text{B1})$$

whereas skyrmions with $\mathcal{G} = 0$ would have a diffusion coefficient of

$$D_{\mathcal{G}=0} = \frac{k_B T}{\alpha \mathcal{D}}. \quad (\text{B2})$$

Here, α is the damping constant and \mathcal{D} is the dissipation. An important quantity for characterizing the strength of the topology is the fraction of the gyrocoupling \mathcal{G} to the skyrmion friction $\alpha \mathcal{D}$, as it is directly related to the skyrmion Hall angle θ [22]:

$$\theta = \arctan\left(\frac{\mathcal{G}}{\alpha \mathcal{D}}\right). \quad (\text{B3})$$

In lattices, we can define effective quantities for the dissipation $\tilde{\mathcal{D}}$, the gyrocoupling $\tilde{\mathcal{G}}$, and skyrmion Hall angle $\tilde{\theta}$.

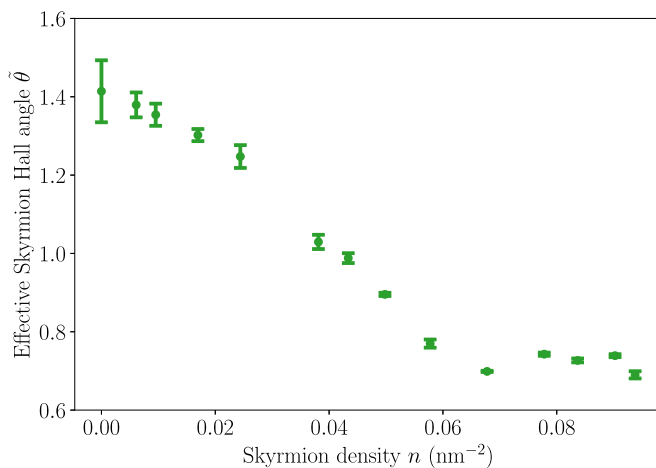


FIG. 6. Effective skyrmion Hall angle $\tilde{\theta}$. Dissipation coefficients were obtained by a linear fit to the time-resolved mean-squared displacement for $\alpha = 0.1$ with and without gyrocoupling, using the same parameters as in Fig. 2 of the main text.

We note that the effective dissipation $\tilde{\mathcal{D}}$ has two distinct factors affecting its particular value. First, the value may change due to neighboring skyrmions distorting its spin configuration. As the dissipation tensor can be calculated as an integral over the spin configuration [43], the value may change as a consequence. We do not take these into account in our simulations. The second source for potential changes in $\tilde{\mathcal{D}}$ comes from the fact that the skyrmions' movement is restricted in a lattice, and thus effective friction is much higher than for free diffusion. By comparing Eq. (B2) to Fig. 2 from the main text, one can see that D decreases exponentially, thus $\tilde{\mathcal{D}}$ increases exponentially with skyrmion density at low densities. In our calculations we assume that skyrmions with different gyrocouplings are affected equally, and thus $\tilde{\mathcal{D}}_{\mathcal{G}\neq 0} = \tilde{\mathcal{D}}_{\mathcal{G}=0}$, which we justify with respect to equal equilibrium properties presented later. Under this assumption, we can calculate

$$\frac{D_{\mathcal{G}=0}}{D_{\tilde{\mathcal{G}}\neq 0}} = \frac{\tilde{\mathcal{G}}^2 + (\alpha \tilde{\mathcal{D}})^2}{(\alpha \tilde{\mathcal{D}})^2} = \left(\frac{\tilde{\mathcal{G}}}{\alpha \tilde{\mathcal{D}}}\right)^2 + 1, \quad (\text{B4})$$

$$\frac{\tilde{\mathcal{G}}}{\alpha \tilde{\mathcal{D}}} = \sqrt{\frac{D_{\mathcal{G}=0}}{D_{\tilde{\mathcal{G}}\neq 0}} - 1}, \quad (\text{B5})$$

and thus we get the effective skyrmion Hall angle

$$\tilde{\theta} = \arctan\sqrt{\frac{D_{\mathcal{G}=0}}{D_{\tilde{\mathcal{G}}\neq 0}} - 1}. \quad (\text{B6})$$

To obtain the diffusion constants, we fitted the time-resolved mean-square displacement data. We note that in the main text we argue that we could not fit all the curves for all densities due to the curves not being exactly linear. While this is true, our method here only requires an approximation of a diffusion constant. The result can be seen in Fig. 6. We observe that for low densities, the skyrmion Hall angle decreases with density, showing that the presence of other skyrmions also affects the skyrmion Hall angle. We did not include the data in the quasicrystalline regime, as the mean-square displacement ceases to increase over time, with the diffusion constant becoming 0 for all systems. The method for calculating the skyrmion Hall angle presented here hence is invalid in that regime.

The skyrmion Hall angle diminishes by about a factor of 2 in our lattices at most. This shows that even though the suppression of diffusion is partially lifted, the effective gyrocoupling $\tilde{\mathcal{G}}$ is not zero. Unlike in the previously discussed case of a one-dimensional harmonic potential, we only see a partial suppression of the topological properties in skyrmion lattices. In Ref. [45], a reduction of the Hall angle to zero is reported for very high densities. While we can confirm a strong reduction in the skyrmion Hall angle, we cannot access the solid phase skyrmion Hall angle with our method, and therefore do not see a reduction to zero.

APPENDIX C: DIFFUSION OF LATTICE DEFECTS

In the main text, we attributed the faster diffusion of larger lattice defects to the more frequent jumps being observed during their motion. We confirm this by calculating the distri-

TABLE I. Probability of observing jumps of topological defects during a time step of 2.416×10^{-5} ns.

	Dislocation pairs	Dislocations	Disclinations
$\mathcal{G} \neq 0$	26.7%	0.192%	4.92×10^{-5}
$\mathcal{G} = 0$	36.5%	1.41%	6.83×10^{-5}

bution of distances traveled in an individual time step of our simulation with $\Delta t = 2.416 \times 10^{-5}$ ns. We find that almost all distance differences are either very small, or at least as large as the distance $d \approx 3.19$ nm, which is the size of the skyrmions. We can formulate a criterion for jumping, with the traveled distance being at least $d/2$, to be considered a jump. The probability of jumping during a single time step for the different topological defects is shown in Table I. With this we can confirm that the larger MSD shown in Fig. 3 of the main text is associated with larger jumping likelihood, and jumping likelihood is increased with the size of the topological defect and the absence of gyrocoupling.

APPENDIX D: MELTING AND FREEZING OF SKYRMION LATTICES

In the main text, we discussed diffusive properties in thermal equilibrium and showed the partial lifting of topological suppression, but did not examine out-of-equilibrium effects. In the following, we show two different nonequilibrium scenarios for skyrmion lattices, where the lifting of topological suppression is a relevant aspect for the time evolution of the entire system. Specifically, we show a system melting from a perfect hexagonal skyrmion lattice, and the freezing of a thermalized skyrmionic system.

As described in the main text, we model the temperature influence as a stochastic force exerted on the individual skyrmions. The force has zero mean and a covariance of $\langle F_{i,\text{th},\mu}(t)F_{j,\text{th},\nu}(t') \rangle = 2\alpha k_B T \mathcal{D}_{\mu\nu} \delta_{ij} \delta(t - t')$. These forces are a result of the skyrmions coupling to the spin heat bath. In our simulations, we assume instantaneous change in this heat-bath temperature, either from low temperatures to high temperatures in the case of melting the skyrmion lattice, or from high to low temperatures for freezing of the skyrmion lattice. We note that while an instantaneous change in the heat-bath temperature is not physically plausible, this choice can be justified since the equilibration of the spin lattice is much faster than the equilibration of the skyrmion lattice system.

In these simulations, we quantify aspects of the orientational order in the system, and how it is affected by the dynamical parameters of the skyrmions. In equilibrium, one can use the orientation correlation function $g_6(t)$ which only depends on the time difference between the two considered configurations. However, since our simulations are not in equilibrium, we have to use different measures. We define

$$g_6(t, t') = \langle \Psi_6(t) \Psi_6^*(t') \rangle$$

as an orientational measure, which relates two specific points in time. The average is over all skyrmions, but not over time. The quantity Ψ_6 is the bond order parameter. Note that $g_6(t, t) = \langle |\Psi_6|^2 \rangle(t)$.

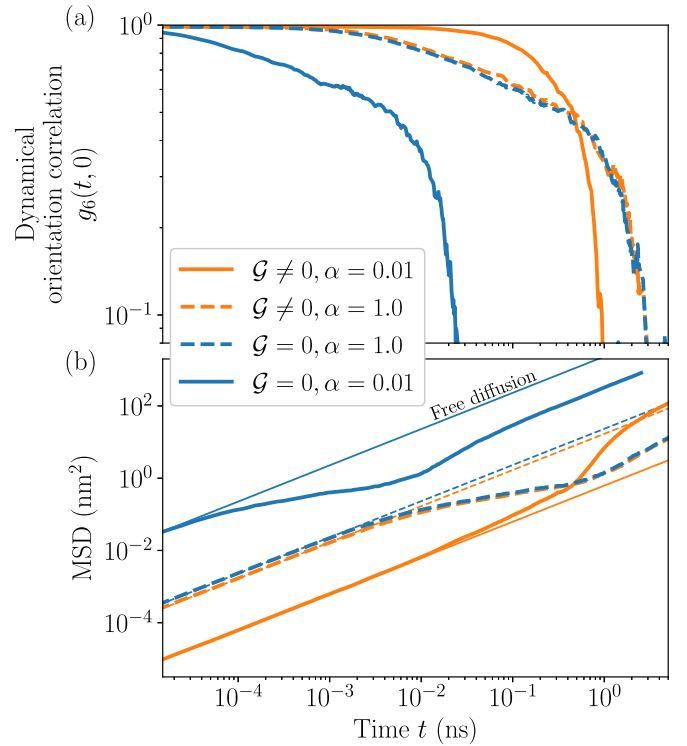


FIG. 7. (a) Dynamical orientation correlation function $g_6(t, 0)$ for the melting process of skyrmion lattices with various combinations of gyrocoupling \mathcal{G} and damping constant α . (b) MSD for a skyrmion lattice in the melting process for various combinations of \mathcal{G} and α . Thin lines indicate analytic calculations for free diffusion for the corresponding curves.

To study the melting process of a skyrmion lattice explicitly, we initialize a perfect hexagonal skyrmion lattice, corresponding to zero temperature, and then simulate the diffusive behavior at constant temperature $T = 20$ K and density $n = 0.09 \text{ nm}^{-2}$ with and without gyrocoupling. The skyrmions in the initial configuration have a distance of 3.58 nm to their nearest neighbor. This combination of temperature and density places the system in the isotropic liquid phase in equilibrium, as demonstrated and discussed in Appendix E. In Fig. 7 we show $g_6(t, 0)$ as well as the MSD of the skyrmions as a function of time with respect to the initially ordered lattice at time $t_0 = 0$. Immediately one observes that the presence or absence of gyrocoupling changes the role of α on the diffusive behavior. While for the high-damping case, $\alpha = 1$, the curves with $\mathcal{G} = 0$ and $\mathcal{G} \neq 0$ are very similar, lowering α leads to clearly distinct behaviors. For $\mathcal{G} = 0$, lowering α simply accelerates the melting process by increasing the diffusive motion of the individual skyrmions. For $\mathcal{G} \neq 0$, the melting process is initially slower, $g_6(t, 0)$ stays at high values for longer, and the MSD is reduced. Only at later times, the melting process speeds up and the MSD reaches values even surpassing the high-damping case. Meanwhile, the orientation correlation falls rapidly, becoming lower than for the high-damping case. This shows that even though the free diffusion of these skyrmions is slower than for skyrmions at high damping, the lattice melts faster.

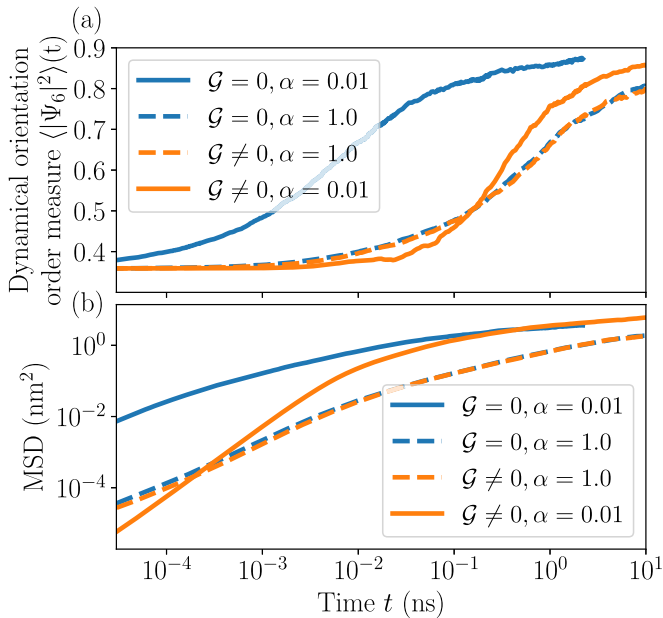


FIG. 8. (a) Orientational order measure $\langle |\Psi_6|^2 \rangle(t)$ for a skyrmion lattice in the freezing process for various combinations of \mathcal{G} and α . (b) MSD for a skyrmion lattice in the freezing process for various combinations of \mathcal{G} and α . The temperature is $T = 1$ K.

As the skyrmions were initialized at a distance close to the minimum of the interaction potential, the MSD initially increases linearly with time with no large influence by the interactions. This is similar to the simulation in a one-dimensional harmonic interaction potential, as there the diffusion constant is initially low, behaving similarly to free diffusion. As soon as the influence of the interactions increases, the $\mathcal{G} = 0$ and $\mathcal{G} \neq 0$ with $\alpha = 1$ cases show a significant reduction in the slope of the MSD, whereas the low-damping case with gyrocoupling shows an enhancement of the diffusion. Note that the changes in the diffusion constant show up as a y offset on the log-log scale, whereas a difference in slopes indicates local subdiffusive or superdiffusive behavior. By direct comparison, the gyrocoupling causes an increase in diffusive behavior in skyrmion lattices compared to free diffusion. However, the diffusion does not surpass the diffusion of skyrmions with $\mathcal{G} = 0$, indicating that the increase of diffusion is the result of the lifting of topological suppression of diffusion.

We now discuss the case of freezing skyrmion lattices and examine the effects of lifting of topological suppression. Figure 8 shows these simulations, which are started in the isotropic liquid phase previously equilibrated at $T = 20$ K. The simulations themselves are performed at $T = 1$ K, which with the density of 0.09 nm^{-2} sets this system in the quasicrystalline phase in equilibrium. In Fig. 8(a), the average bond order $\langle |\Psi_6|^2 \rangle(t)$ is shown. Again, the high-damping case shows little difference between the cases with and without gyrocoupling. Lowering α with $\mathcal{G} = 0$ increases the speed of the freezing process, as $\langle |\Psi_6|^2 \rangle$ increases faster, whereas with $\mathcal{G} \neq 0$, lowering α speeds up the process in the later stages of freezing. Regarding the MSD, one can see that the process of lifting of the topological suppression starts at lower times

compared to the melting process, and $\mathcal{G} \neq 0$ MSD increases up to the level of skyrmions with $\mathcal{G} = 0$. In this case, a complete lifting of topological suppression is observed, but the system is no longer diffusive at long times.

A complete lifting of the topological suppression of diffusion suggests that the skyrmion Hall angle vanishes in these systems. We previously calculated the skyrmion Hall angle for different skyrmion densities in Appendix B, and noticed a decrease in the Hall angle with increasing density. One may also argue that this connection is not simply due to the skyrmion density, but rather very dependent on the phase of the system: As one approaches the quasicrystalline phase, the skyrmion Hall angle decreases, which would be in line with the observation in this particular simulation.

APPENDIX E: EQUILIBRIUM CORRELATION FUNCTIONS

In the main text, we claimed that the spatial correlation functions in equilibrium do not depend on the values of α and \mathcal{G} . We also made claims about an observed phase transition around the steep drop in MSD at a particular density, which we verify using spatial correlation functions in equilibrium. We want to substantiate these claims by showing the pair correlation function $g(r)$ and the spatial orientational correlation function $g_6(r)$. The pair correlation function $g(r)$ in two-dimensions is calculated via

$$g(r) = \frac{A}{4\pi r N^2} \left\langle \sum_i \sum_{j \neq i} \delta(r - r_{ij}) \right\rangle, \quad (\text{E1})$$

where A is the system area, N the number of particles, and r_{ij} the distance between particles i and j . We show the spatial orientational correlation functions for three chosen densities, but different choices for \mathcal{G} and α in Fig. 9. Figure 10 shows the pair correlation functions for the same sets of parameters. The densities were chosen to show three distinct scenarios: A system in the quasicrystalline phase, a system in the liquid phase close to the phase transition, and one in the liquid phase far from the phase transition.

Both figures display nine lines: The same color indicates that the skyrmion density is the same, while the different line styles indicate different choices for the parameters of α and \mathcal{G} . However, it is immediately noticeable that the curves for different line styles overlap each other, confirming that the choice of the parameters for α and \mathcal{G} do not affect the correlation functions in thermal equilibrium, and therefore the phase of the system.

We start by discussing the spatial orientational correlation functions. The blue curves show a clearly finite value for $r \rightarrow \infty$, indicating the quasicrystalline phase. The peaks of the orange curves decay exponentially, which shows liquid behavior, as the local lattice orientation becomes uncorrelated for large distances. For the green curves, only noise can be observed. This is because the system is so far in the liquid phase that the decay of the correlation could not be resolved with our amount of data. This identification of the phases confirms that the drop in MSD in Fig. 2 of the main text is associated with a phase transition.

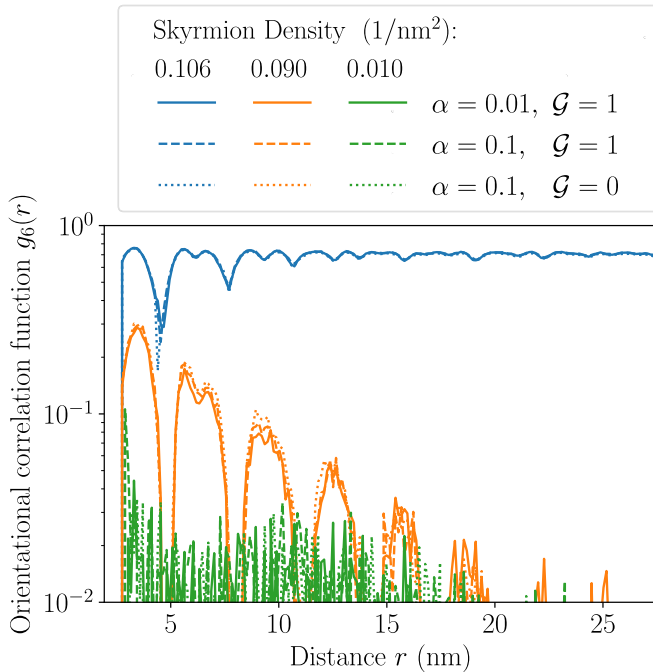


FIG. 9. Spatial orientational correlation function for three chosen skyrmion densities n in thermal equilibrium. The colors indicate density, while line styles show different combinations of α and \mathcal{G} . Solid lines indicate $\mathcal{G} \neq 0$ and $\alpha = 0.01$, dashed for $\mathcal{G} \neq 0$ and $\alpha = 0.1$, and dotted lines for $\mathcal{G} = 0$ and $\alpha = 0.1$.

We also discuss the behavior of the pair correlation functions $g(r)$ in Fig. 10. One should note that a constant value of 1 is associated with an entirely unordered system, while lower or higher values indicate a reduced or increased probability of finding other particles at said distance, respectively. All curves show a value of zero close to a distance of zero, as the particles have a repulsive interaction at short distances. The blue curves show peaks at specific distances, which can be associated with the quasicrystalline phase. Because the

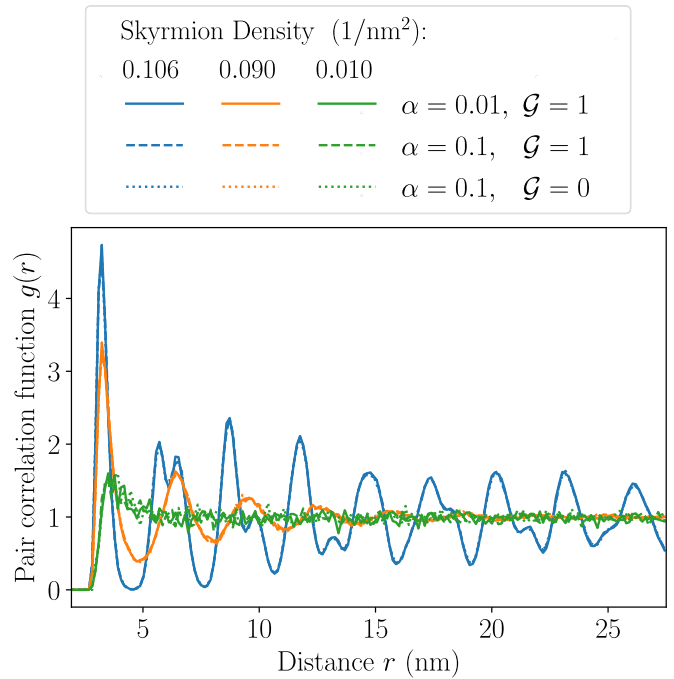


FIG. 10. Pair correlation function for three chosen skyrmion densities n in thermal equilibrium. The colors indicate density, while line styles show different combinations of α and \mathcal{G} . Solid lines indicate $\mathcal{G} \neq 0$ and $\alpha = 0.01$, dashed for $\mathcal{G} \neq 0$ and $\alpha = 0.1$, and dotted lines for $\mathcal{G} = 0$ and $\alpha = 0.1$.

system is two dimensional, no long-range order can exist due to the Mermin-Wagner theorem, and the pair correlation slowly decays to a value of 1 at large distances. As this decay is very slow, one can associate the blue curves with the quasicrystalline phase. The orange curves show a faster decay to 1, with some oscillations around the terminal value. In the green curves, for a system far in the liquid phase, we see a very quick decay to 1 after the initial maximum, indicating an entirely disordered system at relatively small distances.

-
- [1] C. Cisowski, J. B. Götze, and S. Franke-Arnold, Colloquium: Geometric phases of light: Insights from fiber bundle theory, *Rev. Mod. Phys.* **94**, 031001 (2022).
- [2] B. I. Halperin, APS medal for exceptional achievement in research: Topology and other tools in condensed matter physics, *Rev. Mod. Phys.* **92**, 045001 (2020).
- [3] N. D. Mermin, The topological theory of defects in ordered media, *Rev. Mod. Phys.* **51**, 591 (1979).
- [4] H. Arodz, J. Dziarmaga, and W. Zurek, *Patterns of Symmetry Breaking*, Nato Science Series II (Springer, Dordrecht, 2003).
- [5] P. Virnau, Y. Kantor, and M. Kardar, Knots in globule and coil phases of a model polyethylene, *J. Am. Chem. Soc.* **127**, 15102 (2005).
- [6] C. Micheletti, D. Marenduzzo, and E. Orlandini, Polymers with spatial or topological constraints: Theoretical and computational results, *Phys. Rep.* **504**, 1 (2011).
- [7] B. I. Halperin and D. R. Nelson, Theory of two-dimensional melting, *Phys. Rev. Lett.* **41**, 121 (1978).
- [8] N. Nagaosa and Y. Tokura, Topological properties and dynamics of magnetic skyrmions, *Nat. Nanotechnol.* **8**, 899 (2013).
- [9] S. L. Sondhi, A. Karlhede, S. A. Kivelson, and E. H. Rezayi, Skyrmions and the crossover from the integer to fractional quantum Hall effect at small Zeeman energies, *Phys. Rev. B* **47**, 16419 (1993).
- [10] A. Bogdanov and A. Hubert, Thermodynamically stable magnetic vortex states in magnetic crystals, *J. Magn. Magn. Mater.* **138**, 255 (1994).
- [11] S. Mühlbauer, B. Binz, F. Jonietz, C. Pfleiderer, A. Rosch, A. Neubauer, R. Georgii, and P. Böni, Skyrmion lattice in a chiral magnet, *Science* **323**, 915 (2009).
- [12] K. V. Bergmann, A. Kubetzka, O. Pietzsch, and R. Wiesendanger, Interface-induced chiral domain walls, spin spirals and skyrmions revealed by spin-polarized scanning tunneling microscopy, *J. Phys.: Condens. Matter* **26**, 394002 (2014).

- [13] P.-J. Hsu, A. Kubetzka, A. Finco, N. Romming, K. von Bergmann, and R. Wiesendanger, Electric-field-driven switching of individual magnetic skyrmions, *Nat. Nanotechnol.* **12**, 123 (2017).
- [14] A. Fert, V. Cros, and J. Sampaio, Skyrmions on the track, *Nat. Nanotechnol.* **8**, 152 (2013).
- [15] J. Iwasaki, M. Mochizuki, and N. Nagaosa, Current-induced skyrmion dynamics in constricted geometries, *Nat. Nanotechnol.* **8**, 742 (2013).
- [16] Y. Zhou and M. Ezawa, A reversible conversion between a skyrmion and a domain-wall pair in a junction geometry, *Nat. Commun.* **5**, 4652 (2014).
- [17] D. Pinna, F. Abreu Araujo, J.-V. Kim, V. Cros, D. Querlioz, P. Bessiere, J. Droulez, and J. Grollier, Skyrmion gas manipulation for probabilistic computing, *Phys. Rev. Appl.* **9**, 064018 (2018).
- [18] J. Zázvorka, F. Jakobs, D. Heinze, N. Keil, S. Kromin, S. Jaiswal, K. Litzius, G. Jakob, P. Virnau, D. Pinna, K. Everschor-Sitte, L. Rózsa, A. Donges, U. Nowak, and M. Kläui, Thermal skyrmion diffusion used in a reshuffler device, *Nat. Nanotechnol.* **14**, 658 (2019).
- [19] K. Raab, M. A. Brems, G. Beneke, T. Dohi, J. Rothörl, F. Kammerbauer, J. H. Mentink, and M. Kläui, Brownian reservoir computing realized using geometrically confined skyrmion dynamics, *Nat. Commun.* **13**, 6982 (2022).
- [20] M. A. Brems, M. Kläui, and P. Virnau, Circuits and excitations to enable Brownian token-based computing with skyrmions, *Appl. Phys. Lett.* **119**, 132405 (2021).
- [21] A. A. Thiele, Steady-state motion of magnetic domains, *Phys. Rev. Lett.* **30**, 230 (1973).
- [22] W. Jiang, X. Zhang, G. Yu, W. Zhang, X. Wang, M. B. Jungfleisch, J. E. Pearson, X. Cheng, O. Heinonen, K. L. Wang, Y. Zhou, A. Hoffmann, and S. G. E. te Velthuis, Direct observation of the skyrmion Hall effect, *Nat. Phys.* **13**, 162 (2017).
- [23] K. Litzius, I. Lemesh, B. Krüger, P. Bassirian, L. Caretta, K. Richter, F. Büttner, K. Sato, O. A. Tretiakov, J. Förster, R. M. Reeve, M. Weigand, I. Bykova, H. Stoll, G. Schütz, G. S. D. Beach, and M. Kläui, Skyrmion Hall effect revealed by direct time-resolved x-ray microscopy, *Nat. Phys.* **13**, 170 (2017).
- [24] C. Schütte, J. Iwasaki, A. Rosch, and N. Nagaosa, Inertia, diffusion, and dynamics of a driven skyrmion, *Phys. Rev. B* **90**, 174434 (2014).
- [25] X. Z. Yu, Y. Onose, N. Kanazawa, J. H. Park, J. H. Han, Y. Matsui, N. Nagaosa, and Y. Tokura, Real-space observation of a two-dimensional skyrmion crystal, *Nature (London)* **465**, 901 (2010).
- [26] X. Z. Yu, N. Kanazawa, Y. Onose, K. Kimoto, W. Z. Zhang, S. Ishiwata, Y. Matsui, and Y. Tokura, Near room-temperature formation of a skyrmion crystal in thin-films of the helimagnet FeGe, *Nat. Mater.* **10**, 106 (2011).
- [27] P. Huang, T. Schönenberger, M. Cantoni, L. Heinen, A. Magrez, A. Rosch, F. Carbone, and H. M. Rønnow, Melting of a skyrmion lattice to a skyrmion liquid via a hexatic phase, *Nat. Nanotechnol.* **15**, 761 (2020).
- [28] J. Zázvorka, F. Dittrich, Y. Ge, N. Kerber, K. Raab, T. Winkler, K. Litzius, M. Veis, P. Virnau, and M. Kläui, Skyrmion lattice phases in thin film multilayer, *Adv. Funct. Mater.* **30**, 2004037 (2020).
- [29] C. A. Murray and D. H. Van Winkle, Experimental observation of two-stage melting in a classical two-dimensional screened Coulomb system, *Phys. Rev. Lett.* **58**, 1200 (1987).
- [30] A. H. Marcus, B. Lin, and S. A. Rice, Self-diffusion in dilute quasi-two-dimensional hard sphere suspensions: Evanescent wave light scattering and video microscopy studies, *Phys. Rev. E* **53**, 1765 (1996).
- [31] A. H. Marcus and S. A. Rice, Phase transitions in a confined quasi-two-dimensional colloid suspension, *Phys. Rev. E* **55**, 637 (1997).
- [32] U. Gasser, C. Eisenmann, G. Maret, and P. Keim, Melting of crystals in two dimensions, *Chem. Phys. Chem.* **11**, 963 (2010).
- [33] S. Deuschländer, P. Dillmann, G. Maret, and P. Keim, Kibble-Zurek mechanism in colloidal monolayers, *Proc. Natl. Acad. Sci. USA* **112**, 6925 (2015).
- [34] J. M. Kosterlitz and D. J. Thouless, Ordering, metastability and phase transitions in two-dimensional systems, *J. Phys. C: Solid State Phys.* **6**, 1181 (1973).
- [35] D. R. Nelson and B. I. Halperin, Dislocation-mediated melting in two dimensions, *Phys. Rev. B* **19**, 2457 (1979).
- [36] A. P. Young, Melting and the vector Coulomb gas in two dimensions, *Phys. Rev. B* **19**, 1855 (1979).
- [37] A. Pertsinidis and X. S. Ling, Diffusion of point defects in two-dimensional colloidal crystals, *Nature (London)* **413**, 147 (2001).
- [38] P. Lipowsky, M. J. Bowick, J. H. Meinke, D. R. Nelson, and A. R. Bausch, Direct visualization of dislocation dynamics in grain-boundary scars, *Nat. Mater.* **4**, 407 (2005).
- [39] A. Libál, C. Reichhardt, and C. J. Olson Reichhardt, Point-defect dynamics in two-dimensional colloidal crystals, *Phys. Rev. E* **75**, 011403 (2007).
- [40] S.-C. Kim, L. Yu, A. Pertsinidis, and X. S. Ling, Dynamical processes of interstitial diffusion in a two-dimensional colloidal crystal, *Proc. Natl. Acad. Sci. USA* **117**, 13220 (2020).
- [41] Y. Ge, J. Rothörl, M. A. Brems, N. Kerber, R. Gruber, T. Dohi, M. Kläui, and P. Virnau, Constructing coarse-grained skyrmion potentials from experimental data with iterative Boltzmann inversion, *Commun. Phys.* **6**, 30 (2023).
- [42] S. Deuschländer, T. Horn, H. Löwen, G. Maret, and P. Keim, Two-dimensional melting under quenched disorder, *Phys. Rev. Lett.* **111**, 098301 (2013).
- [43] M. Weißenhofer and U. Nowak, Diffusion of skyrmions: The role of topology and anisotropy, *New J. Phys.* **22**, 103059 (2020).
- [44] E. Kalz, H. D. Vuijk, I. Abdoli, J.-U. Sommer, H. Löwen, and A. Sharma, Collisions enhance self-diffusion in odd-diffusive systems, *Phys. Rev. Lett.* **129**, 090601 (2022).
- [45] C. J. O. Reichhardt and C. Reichhardt, Active rheology in odd-viscosity systems, *Europhys. Lett.* **137**, 66004 (2022).
- [46] Y.-W. Li and M. P. Ciamarra, Phase behavior of Lennard-Jones particles in two dimensions, *Phys. Rev. E* **102**, 062101 (2020).
- [47] S. C. Kapfer and W. Krauth, Two-dimensional melting: From liquid-hexatic coexistence to continuous transitions, *Phys. Rev. Lett.* **114**, 035702 (2015).
- [48] L. Rózsa, A. Deák, E. Simon, R. Yanes, L. Udvardi, L. Szunyogh, and U. Nowak, Skyrmions with attractive interactions in an ultrathin magnetic film, *Phys. Rev. Lett.* **117**, 157205 (2016).

- [49] D. Capic, D. A. Garanin, and E. M. Chudnovsky, Skyrmion–skyrmion interaction in a magnetic film, *J. Phys.: Condens. Matter* **32**, 415803 (2020).
- [50] R. Brearton, G. van der Laan, and T. Hesjedal, Magnetic skyrmion interactions in the micromagnetic framework, *Phys. Rev. B* **101**, 134422 (2020).
- [51] M. Weißenhofer, L. Rózsa, and U. Nowak, Skyrmion dynamics at finite temperatures: Beyond Thiele’s equation, *Phys. Rev. Lett.* **127**, 047203 (2021).
- [52] R. E. Troncoso and Á. S. Núñez, Brownian motion of massive skyrmions in magnetic thin films, *Ann. Phys.* **351**, 850 (2014).
- [53] J. Miltat, S. Rohart, and A. Thiaville, Brownian motion of magnetic domain walls and skyrmions, and their diffusion constants, *Phys. Rev. B* **97**, 214426 (2018).
- [54] H. Lowen and G. Szamel, Long-time self-diffusion coefficient in colloidal suspensions: Theory versus simulation, *J. Phys.: Condens. Matter* **5**, 2295 (1993).
- [55] C. Reichhardt, C. J. O. Reichhardt, and M. V. Milošević, Statics and dynamics of skyrmions interacting with disorder and nanostructures, *Rev. Mod. Phys.* **94**, 035005 (2022).
- [56] L. Kong, X. Chen, W. Wang, D. Song, and H. Du, Dynamics of interstitial skyrmions in the presence of temperature gradients, *Phys. Rev. B* **104**, 214407 (2021).
- [57] M. Weißenhofer, Stochastic and deterministic dynamics of topological spin textures: Theory and simulation, Ph.D. thesis, Universität Konstanz, Konstanz, 2022.
- [58] B. Øksendal, *Stochastic Differential Equations: An Introduction with Applications* (Springer, Berlin, 2000), Vol. 82.